Chapter- 4

Repurposing of potential anti-parasitic inhibitors against specific *Leishmania* protein targets

4.1. Abstract

Leishmania donovani, an obligatory intracellular flagellate pathogen, is the underlying cause of VL, a fatal disease that poses a significant challenge to existing therapeutic approaches and leads to human mortality. In an endeavor to find an antileishmanial drug to combat VL, we aimed to assess the approved drug molecules against the specific drug targets of VL. In this study, a theoretical method was used to select two essential therapeutic targets (pyridoxal kinase [PK] and sterol alpha-14 demethylase [SDM]) which were present in both the data set of essential genes and drug target proteins. The selected PK and SDM proteins in *L. donovani* play pivotal roles as essential enzymes in the crucial vitamin B6 salvage and sterol biosynthesis pathways, respectively, leading to pathogenicity in humans. In addition to that drugs were gathered from the DrugBank and DrugCentral databases and 325 (out of 4867) compounds having anti-parasitic properties were screened by PASS analysis. Consequently, three ligands Lig_1 [Nitazoxanide (PubChem ID-41684)], Lig_2 [Fenclofenac (PubChem ID-65394)] and Lig_3 [Artemisinin (PubChem ID-68827)] were chosen based on their elevated Pa values, docking scores, and notable medicinal applications. Moreover, the result obtained from MD simulation suggests Lig_1 does not affect the structural integrity of both targets. Additionally, evaluation of total binding energies by MMPBSA analyses showed stronger binding of Lig_1 with PK and SDM is -100.71 and -175.61 kJ/mol, respectively compared to others. As a whole, the methodology employed in this research involves the simultaneous identification of suitable protein targets and potential inhibitors. Through this investigation, we have demonstrated that compounds derived from a biocomputing approach exhibit interaction mechanisms as inhibitors against drug targets, offering a promising avenue for addressing VL.

In this chapter, Lig_1, Lig_2 and Lig_3 is considered as Nitazoxanide, Fenclofenac and Artemisinin, respectively.

4.2. Introduction

Leishmaniasis, a disease transmitted by vectors, is caused by protozoa characterized by a hemoflagellate structure. This ailment poses a significant global public health challenge as

a zoonotic condition. It is categorized as a neglected tropical disease due to the insufficient focus on its infection. The impact of the *Leishmania* pathogen is predominantly evident in countries such as India, Nepal, Bangladesh, Ethiopia, Sudan, Kenya, and others. These nations, mostly characterized as underdeveloped, experience substantial repercussions, thereby influencing their progress and development. Furthermore, these parasites are prevalent in countries situated within tropical and temperate zones [1]. The World Health Organization (WHO) has documented *Leishmania* parasite infections in approximately 12 million individuals. The most severe and lethal form of leishmaniasis is VL, better known as kala-azar in India [2]. The primary cause of VL is attributed to *Leishmania donovani*, a protozoan organism that exists in two distinct forms: promastigote and amastigote. *L. donovani* needs both humans and sand flies as hosts for the successful completion of life cycle. In this context, when an infected sandfly bites a human, it transmits the pathogen into the human body, enabling the completion of the remaining portion of its life cycle. During this life cycle phase, the parasites start exerting their impact on humans, ultimately resulting in the demise of the host. [3, 4]. This pathogen's life cycle gives information about the infective stage, which aids in prevention and development of therapies against the pathogen.

The treatment of visceral leishmaniasis relies solely on chemical compounds as medications. The present therapeutic options for leishmaniasis encompass miltefosine, paromomycin, and AmpB [5]. To develop new medications, diverse methodologies have been introduced over time, including systems biology approaches [6], kinetic modelling approaches [7], multi-target approaches [8], etc. Various fields within computational biology have emerged, providing numerous avenues for exploration, in the quest to discover efficient medications that combat diseases such as cancer, malaria, COVID-19, and more [9, 10]. Since there is currently no vaccine for VL, there is an urgent need for a vaccine or medication. Hence, there is a need for an innovative method to identify molecular targets, enhancing treatment strategies that can effectively inhibit or eliminate the parasites responsible for VL, all while ensuring the safety of human hosts.

Essential genes indicate their absolute indispensability for the growth and survival of the organism. They are, in other words, vital for the existence and viability of an organism. According to previous research, the majority of essential genes, are involved in homeostasis, DNA replication, damage repair, etc. [11, 12]. Previous research on various pathogens, including *Pseudomonas aeruginosa*, Epstein–Barr virus and *Leishmania*, have been targeted via drug development approaches [13-15]. As a result, determining the targets for

pharmacological treatments will help to simplify things in the fields of molecular pharmacology and medication efficacy [16, 17].

Vitamins are essential nutrients that serve as co-enzymes within the pathogen, thus playing a vital role in supporting various metabolism. Among these, pyridoxal-5'-phosphate or vitamin B6 is recognized as a crucial vitamin necessary for the growth and development of microorganisms. In this regard, vitamin B6 is associated with various functions like synthesis of neurotransmitters, elimination reactions, decarboxylation, etc. [18, 19]. Nevertheless, diverse forms of vitamin B6 encompass pyridoxal (PL), pyridoxamine (PM), and pyridoxine (PN), all of which are acquired from the host's body and subsequently transformed into distinct forms by *Leishmania* species. Pyridoxal kinase (PK) catalyzes the phosphorylation of the 5′ hydroxyl group of PL to form PL [20]. Inhibitors of PK are regarded as promising drug candidates for the treatment of protozoan infectious illnesses because these drug targets play a crucial role in vitamin B6 metabolism in cells [21, 22]. In the cases of *Trypanosoma brucei* and *Plasmodium falciparum*, PK has been identified as a potential drug target due to its essential role in the survival and pathogenicity of the parasites [23]. Various investigations focused on leishmanial PK have asserted its ability to impede the propagation of infection and the proliferation of the pathogen [20, 24]. The significant involvement of *L. donovani* PK in the vitamin B6 pathway identifies it as a promising target for interventions against leishmanial infections.

Sterol biosynthesis is a metabolic pathway found to be involved in the formation of cell membranes in various organisms [25]. Ergosterol and ergosterol-like sterols of cell membranes are found in *Leishmania* and *Trypanosoma*, and fungi, respectively whereas cholesterol is found in the cell wall of humans for performing functions like fluidity of membrane, membrane permeability, etc. In this regard, sterol biosynthesis is crucial of cell membrane formation in *L. donovani*. However, variations in the types of sterols result in distinct cell membrane compositions among different organisms [26]. The human plasma membrane serves as a route for *Leishmania* to gain entry into human cells. Additionally, the lipid raft present within this membrane contributes to the parasite's virulence. [27, 28]. In the process of sterol biosynthesis in *Leishmania*, the enzyme sterol alpha-14 demethylase (SDM) holds significant importance as it is responsible for demethylating the C14 ring system [28]. The sterol biosynthesis pathway of *L. donovani* includes the SDM enzyme, which is vital for the survival and growth of the pathogen [29, 30]. Inhibiting SDM results in the disruption of the parasites' membrane integrity, causing the sterol biosynthesis

function to cease, consequently hindering the growth of the *Leishmania* pathogen [31]. The severity of the illness brought on by *L. donovani* and the significance of SDM on sterol biosynthesis made it a pharmacological target for discovering new drugs against VL. Sterol alpha-14 demethylase is usually known as CYP51 but we have used SDM as an abbreviation in this work.

The distinctive aspect of this study is its use of compiled lists of essential genes and drug targets specific to *L. donovani*, enabling the identification of crucial targets. Furthermore, a dataset of drugs is employed to find potential inhibitors against these protein targets, all through the *in-silico* method. We focused on obtaining of essential genes, and reported drug targets of *L. donovani* from relevant literature. Subsequently, common and important protein targets were selected from essential genes and known drug targets of *L. donovani*. The analysis led to the selection of pyridoxal kinase and sterol alpha-14 demethylase as the chosen proteins. The structure of SDM protein was modelled in order to get the structure required for the work. The binding interactions between ligands and amino acid residues are addressed by *in-silico* analyses using various compounds on *L. donovani*, employing the selected proteins. Most of the drugs are a product of different plants which are used in day-to-day life or can be obtained in an around us [32]. Phytochemicals offer the advantage of causing fewer side effects, being more user-friendly, and being cost-effective. This makes them promising candidates for future drug development. The collected drugs were narrowed down on the basis of PASS analysis, which were later proceeded for docking with both proteins. In order to identify potential candidates for VL inhibition, molecular dynamics simulations were performed for selected protein-ligand complexes (Figure 4.1). By undertaking this approach, a comprehensive understanding of the interactions between drug targets and ligands were obtained. Additionally, it also showcases how the ligands influence the protein structures.

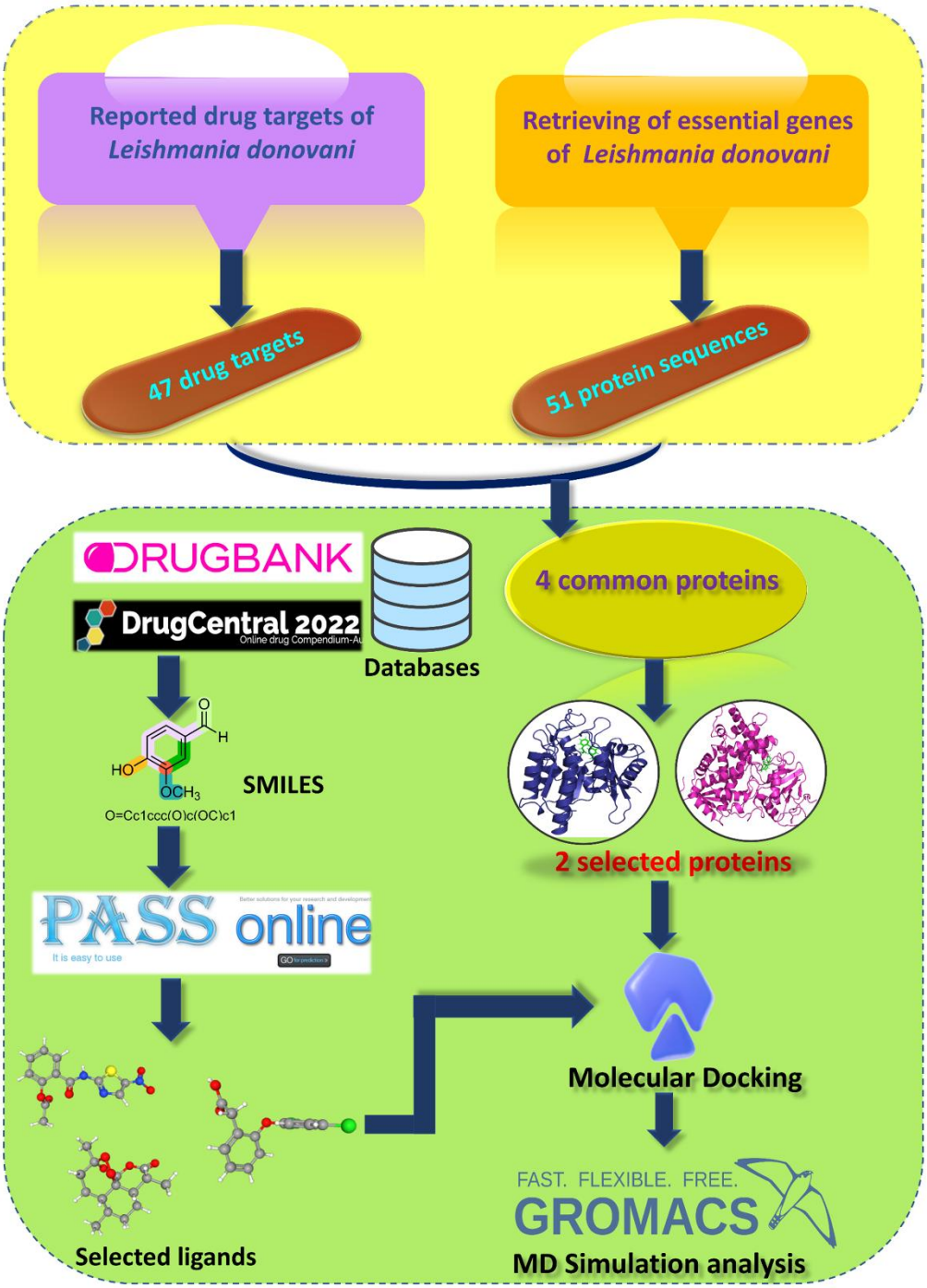

Figure 4.1: Systematic diagram for identifying possible inhibitors against PK and SDM drug targets.

4.3. Methodology

4.3.1. Protein selection and ligand collection

After conducting an extensive review of the literature concerning drug targets and essential genes in *L. donovani*, a compilation of 47 therapeutic targets and 51 essential proteins associated with the essential genes of *L. donovani* was assembled. From the above sets of

data, protein PK and SDM were found to be common in the two protein datasets and chosen as targets. The 3D *L. donovani* protein structures that were available in the RCSB PDB were chosen [33]. In the PDB database, among the available three-dimensional structures of pyridoxal kinase protein from *L. donovani*, four entries were found. Nonetheless, for the present investigation, only a single structure marked by the PDB ID 6K92, notable for its high-resolution quality (1.85Å), was selected. The X-ray diffraction method was employed to acquire the three-dimensional structure having PDB ID- 6K92. The selected PDB ID of PK is a homodimer and has a molecular weight of 36.2kDa and its UniProt (accession id: A0A3S7X3C0). The three-dimensional structure of PK of *L. donovani* contains missing residues in both the chains. To attain a complete protein structure, chain A was selected for modeling due to its relatively lower count of 11 missing residues compared to the other chain. The selected chain A was modeled utilizing software (MODELLER 10.1) by employing a template structure as a reference [34]. On the contrary, the UniProt ID of SDM protein in *L. donovani* is A0A6J8F9Q1; however, this protein lacks a corresponding PDB ID associated with a known three-dimensional structure. Consequently, the structure of the SDM protein from *L. donovani* was computationally modeled using the structure of the SDM protein from *L. infantum* (PDB ID 3L4D and UniProt ID A2TEF2) as a template due to the high percentage sequence identity (93.5%) between them. The modelling of SDM protein was also performed by MODELLER 10.1 software which was further minimized. The molecular weight of SDM of *L. donovani* is about 54 kDa. For the ligand selection, the DrugBank [35] and Drug Central [36] databases were used to compile the list of drugs that represent ligands. Later, the drug's structure-data file was obtained from the PubChem database [37] and transformed into protein data bank format using the Open Babel program [38].

4.3.2. Screening of ligands

This study aims to reuse the current medications for the treatment of VL. To be eligible for consideration in VL treatment, these drugs need to exhibit antiparasitic attributes. The biological activity of the gathered drugs was forecasted through the utilization of PASS (Prediction of Activity Spectra for Biologically Active Substances) analysis. The estimation of biological activity was conducted using structural-activity relationships and these results are cataloged in the PASS database [39]. Activities were forecast as probabilities. The estimated Pa value of molecules with antiparasitic activity was obtained using the PASS online service, and the molecules were then screened based on the Pa value.

4.3.3. Molecular docking studies

The molecular docking was performed by AutoDock 4.2. The selected ligands were docked into the active site of the proteins. A varied grid size of 60 X 56 X 50 for PK and 50 X 58 X 50 for SDM in respect to Å unit with a fixed grid spacing of 0.375Å was used. Ten confirmations of the protein-ligand combination were produced after docking and from them the best docking pose was selected based on the position of ligand with in the active sites of protein and docking score [40].

4.3.4. Molecular Dynamics Simulations

MD simulation enables a time-dependent comprehension of the dynamic characteristics of biological macromolecules and ligands. This approach emulates the atomic positions in a cellular situation, which aids in understanding their behaviour and stability [41]. GROMACS v.2020.4 (GROningen MAchine for Chemical Simulations), a programme that simulates proteins, was used to run a MD simulation [42]. The specifications of the GROMOS 54A7 force field were employed to study the biomolecular systems. Periodic boundary conditions, LINCS algorithm and Simple Point Charge (SPC) water model which were used for the simulation purpose. The PK system had roughly 55,000 atoms and the SDM system had about 1,10,000 atoms. Initially, the system undergoes energy minimization to attain its lowest energy conformation. Detailed processes of MD simulation were employed in Chapter 2.

4.3.5. Binding energy calculations

To determine the role of the residues in governing the interaction between the protein and ligand, binding free energy (BE) calculations must be done post-simulations. With the use of the g_mmpbsa tool, the MMPBSA (Molecular Mechanics Poisson-Boltzmann Surface Area) technique was applied [43].

4.4. Results

In this investigation to identify potential drug targets for visceral leishmaniasis using a biocomputational approach, two sets of data comprising essential genes and drug targets were gathered. The first dataset contained the known 47 pharmaceutical targets of *L. donovani* which are represented in Table 4.1, and the second dataset contained the known 51 essential genes of *L. donovani* which are shown in Table 4.2. From the two dataset, 4 common proteins were obtained, which were later streamlined to 2 proteins i.e., PK and

SDM which have less sequence identity with human homologs protein and are important for the survival of the pathogen. To refine the group of 4867 compounds, a PASS analysis was utilized to identify those with anticipated antiparasitic effects. To gain a more comprehensive insight into the research, two specific drug targets were subjected to docking and molecular dynamics simulations. These simulations were conducted both in the presence and absence of ligands to provide a detailed understanding of the interactions. Moreover, in the end, the binding energy of protein-ligand complexes were computed to further show the interaction reliability.

Table 4.1: Drug targets of *Leishmania donovani* with UniProt ID

Sl. No.	Drug target	UniProt ID
1	Trypanothione reductase	P39050
2	Fumarate reductase	E9BRZ6
3	Cytochrome C oxidase	B7TYN7
4	3-hydroxy-3-methylglutaryl-CoA (HMGCoA) reductase	I7CKJ5
5	Fatty acyl-CoA ligase	---------
6	Sterol methyl transferase	Q6RW42
7	Sterol 14 alpha demethylase	A0A6J8F9Q1
8	Ornithine decarboylase	P27116
9	Spermidine synthase	Q9GSR3
10	Trypanothione synthetase	G5D5D5
11	Deoxyhypusine synthase	B5APK2
12	Deoxyhypusine hydroxylase	D9IFD5
13	Pteridine reductase 1	Q6QDB5
14	Ubiquitin fold modifier-1	A0A504XR09
15	Xanthine phosphoribosyltransferase	Q9U6Y2
16	Hypoxanthine-guanine phosphoribosyl transferase	P43152
17	Adenine phosphoribosyl transferase	Q27679
18	Topoisomerase I	A0A3Q8IHS4
19	Topoisomerase II	A0A3S7WTK8
20	N-myristoyltransferase	D0AB09
21	O-Acetyl serine sulfhydrylase	G1C2I2
22	Dihydroorate dehydrogenase	D0VWT2

23	Pyridoxal Kinase	A0A0G2YFI9
24	Cyclophilin A	Q9U9R3
25	UMP synthase	E9BCQ9
26	Adenylosuccinate lyase	A7LBL3
27	Enolase	--------
28	Squalene synthase	Q257D4
29	MAPK1	--------
30	MAPK3	--------
31	MAPK4	--------
32	Iron superoxide dismutase A	E9BNU5
33	Serine hydroxymethyltransferase	E9BJX3
34	Nicotinamidase	A0A3S5H4V3
35	S-adenosylmethionine decarboxylase	Q25264
36	Arginase	Q0ZAG5
37	Pyruvate phosphate dikinase	A0A3Q8I917
38	Casein Kinase 1	G9FXV0
39	Glyoxalase I	--------
40	Glyoxalase II	E9BAZ7
41	Tryrparedoxin peroxidase	E9BCF2
42	Nucleoside diphosphate kinase b	A0A3S7X5X3
43	Protein disulfide isomerase	B3VA16
44	Ascorbate Peroxidase	H6V7N3
45	L-asparaginase	A0A6J8F6L6
46	Oxidosqualene cyclase	--------
47	Dihydrofolate reductase-thymidylate synthase	E9B8U9

Table 4.2: Essential genes of *Leishmania donovani* with their respective UniProt ID

Sl. No.	Essential genes	UniProt ID
1	Ornithine decarboxylase	E9BB03
2	Spermidine synthase	E9B822
3	5'a2rel-related protein	E9BFT5
4	S-adenosylmethionine decarboxylase proenzyme	E9BM58

5	Lactoylglutathione lyase	E9BSH6
6	Coronin	E9BGF4
7	Deoxyhypusine synthase family protein	E9BQI9
8	Myosin XXI	E9BPF2
9	Orotidine-5-phosphate decarboxylase	E9BCQ6
10	Uracil phosphoribosyl transferase	E9BQR2
11	Hs1vu complex proteolytic subunit-like	E9BUC6
12	Heat shock protein HslVU, ATPase subunit	E9BC50
13	Nitroreductase like protein	E9BI91
14	Arginosuccinate synthase	E9BCR2
15	Asparagine synthetase a, putative	E9BI91
16	Actin-like protein, putative	E9BBF8
17	Protein kinase, putative	E9BE09
18	Ras-related protein rab-5, putative	E9BDU4
19	Small Rab GTP binding protein, putative	E9BG78
20	Acetyl-coenzyme A synthetase	E9BG78
21	Lysine--tRNA ligase	E9BC68
22	10 kDa heat shock protein, putative	E9BI72
23	Threonine--tRNA ligase	E9BS18
24	Hypoxanthine-guanine phosphoribosyl transferase	E9BF84
25	6-phosphogluconolactonase	E9BIT4
26	Acetyl-CoA carboxylase	E9BN78
27	CDP diacylglycerol-serine phosphatidyl transferase	E9BC10
28	Phosphatidate cytidylyltransferase	E9BIH2
29	Phosphatidylinositol synthase	E9BIR1
30	Phosphatidylserine decarboxylase	E9BSY5
31	Enolase-phosphatase E-1	E9BUX4
32	5'-methylthioadenosine phosphorylase	E9B8H3
33	Nicotinate-nucleotidylyl transferase	E9BDG7
34	ATP synthase, epsilon chain, putative	E9BMA9
35	ATP synthase F1 subunit gamma protein, putative	E9BFK0
36	Phosphogluconate dehydrogenase	E9BSL0

37	Trypanothione reductase	E9B8C5
38	Adenine phosphoribosyl transferase	E9BI25
39	Nucleoside-diphosphate kinase	E9BSR1
40	Dihydoorotic acid dehydrogenase	E9BCQ7
41	Dihydroorotase	E9BCR1
42	C-s24 sterol reductase	E9BQ02
43	C-3 sterol dehydrogenase	E9B8P6
44	Farnesyl pyrophosphate synthase	E9BFY6
45	Squalene epoxidase	E9BBL0
46	Sterol 14-demethylase	E9BAU8
47	Amino acid transporter, putative	E9BP31
48	Amino acid permease 3	E9BML5
49	Pyridoxal kinase	E9BLM4
50	Sterol 14alpha-demethylase	C5MLW7
51	N-myristoyltransferase	D0AB09

Table 4.3: List of essential protein present on essential pathway of *L. donovani.*

Sl. No.	**Name of the essential protein**	**Essential pathway of *L. donovani***	**Reference**
1	Sterol-14-alpha demethylase	Sterol biosynthetic pathway	[29,30]
2	Enolase	Glycolytic pathway	[44]
3	Ornithine decarboxylase	Polyamine biosynthesis	[45]
4	S-adenosyl methionine decarboxylase	Polyamine biosynthesis	[46]
5	Spermidine synthase	Hypusine pathway	[47]
6	Trypanothione reductase	Redox metabolism	.[47]
7	Pyridoxal kinase	Vitamin B synthesis pathway	[20]
8	Dihydroorotase	Purine salvage pathway	[48]
9	Hypoxanthine-guanine phosphoribosyl transferase	Purine salvage pathway	[49]

4.4.1. Details of Pyridoxal kinase and Sterol 14-alpha demethylase protein sequences

The protein sequence of PK in *L. donovani* consists of 303 amino acids, whereas the corresponding sequence in humans is longer with 312 amino acids. In addition, the gene encoding PK in *L. donovani* is located on Chromosome 30. However, the level of similarity between the PK protein of *L. donovani* and humans is around 36%. In the case of *Trypanosoma brucei*, the importance of PK was highlighted by observing knockout parasites that were unable to survive in a medium lacking PLP (pyridoxal 5'-phosphate), indicating the essential role of PK in their growth and developmental processes [21]. When mice are subjected to the PK mutant of *T. brucei*, a reduced infection rate is observed among the mice. This outcome underscores the critical role of PK in the parasite's ability to multiply and spread within the host [50]. The active site area of PK in humans and *L. donovani* differs significantly, which highlights PK as a potential target for antileishmanial drugs [20]. Moreover, the amino acid sequence of SDM protein in *L. donovani* and human exhibit a sequence similarity of 35%. The human SDM protein comprises 461 amino acids, while its counterpart in *L. donovani* is longer, consisting of 480 amino acids. The gene responsible for encoding the SDM protein in *L. donovani* is located on chromosome 11. According to reports, a strain lacking SDM was more successful in inhibiting pathogens, proving that SDM is crucial for *L. donovani* [29]. The MODELLER 10.1 software produced five model structures for each case and based on the lowest DOPE (Discrete Optimized Protein Energy) score, one structure for each protein was selected and energy minimized for the docking analysis. The DOPE score of the generated model structures is depicted in Table 4.4.

Table 4.4: Details of modeled structures for PK and SDM protein

Sl. No.	MODEL	DOPE Score	MODEL	DOPE Score
1	PK.B99990001.pdb	-35202.86	SDM.B99990001.pdb	-55564.47
2	PK.B99990002.pdb	-34425.34	SDM.B99990002.pdb	-55494.77
3	PK.B99990003.pdb	-35009.27	SDM.B99990003.pdb	-56477.77
4	PK.B99990004.pdb	-35333.07	SDM.B99990004.pdb	-55206.34
5	PK.B99990005.pdb	-34949.83	SDM.B99990005.pdb	-55466.28

4.4.2. Ligands screening and analysis

In the course of our study, 4867 medicinal molecules were gathered from two distinct databases, and PASS analysis was carried out for them by utilizing the PASS online server. From the total compounds collected, antiparasitic activity was shown by only 325 compounds which have the probability of activity (Pa) value ≥ 0.5 was prepared. Out of 325 ligands, 137, 63, 52, 43, and 30 number of drug molecules fall within the range of Pa values of 0.5-0.59, 0.6-0.69, 0.7-0.79, 0.8-0.89, and 0.9-1.0, respectively and they were considered further for our study.

4.4.3. Molecular docking analysis

For this purpose, AutoDock 4.2 software was utilized, and the program was executed using Lamarckian genetic algorithms (LGA). A comprehensive list of 325 ligands along with their respective PASS scores and docking scores for both proteins was prepared. From the top 10 ranking poses obtained after docking, the conformers with the lowest binding energy were picked. Using the PyMOL platform, the protein-ligand complexes resulting from the docking process were visualized. This visualization aimed to confirm the molecular arrangement within the intended binding site. The active site of PK was defined by specific residues: Ser12, Lys187, Tyr226, Thr229, Gly230 and Asp231. On the other hand, the active site of SDM was characterized by the residues Tyr102, Tyr115, Met357 and Met459. First, two datasets of the top 25 docking scores of PK and SDM with ligands were prepared then from them further screening was done. Table 4.5 presents a compilation of 10 commonly observed ligands from two datasets, which demonstrated high docking scores. From the provided table, three ligands were selected due to their elevated Pa value, favorable docking scores, and established applications as drug candidates. Figure 4.2 showed docked structure of PK and SDM with three selected ligands. To visualize the interactions within the complexes, the Discovery Studio visualization tool was employed.

Table 4.5: PASS analysis, docking result of both proteins with 10 molecules and its common uses

Serial No.	PubChem CID	PASS analysis (Pa Value)	Docking Score (kcal/mol)		Common uses
			PK	SDM	
1	13791	0.520	-5.89	-7.03	Steroid ester
2	33919	0.538	-5.22	-7.14	Skin moisturization and sunscreen
3	41684	0.670	-5.45	-7.58	Antimicrobial & antiviral agent
4	65394	0.531	-5.41	-7.39	Rheumatoid arthritis
5	65588	0.539	-5.19	-7.88	Corticosteroid hormone
6	68827	0.960	-5.29	-7.95	Antimalarial
7	1549120	0.564	-5.1	-7.18	Breast cancer
8	5284553	0.562	-6.36	-7.41	Vasodilator
9	9571044	0.523	-6.27	-7.18	Anti-infectious agent
10	10360683	0.596	-5.79	-7.42	Androgen

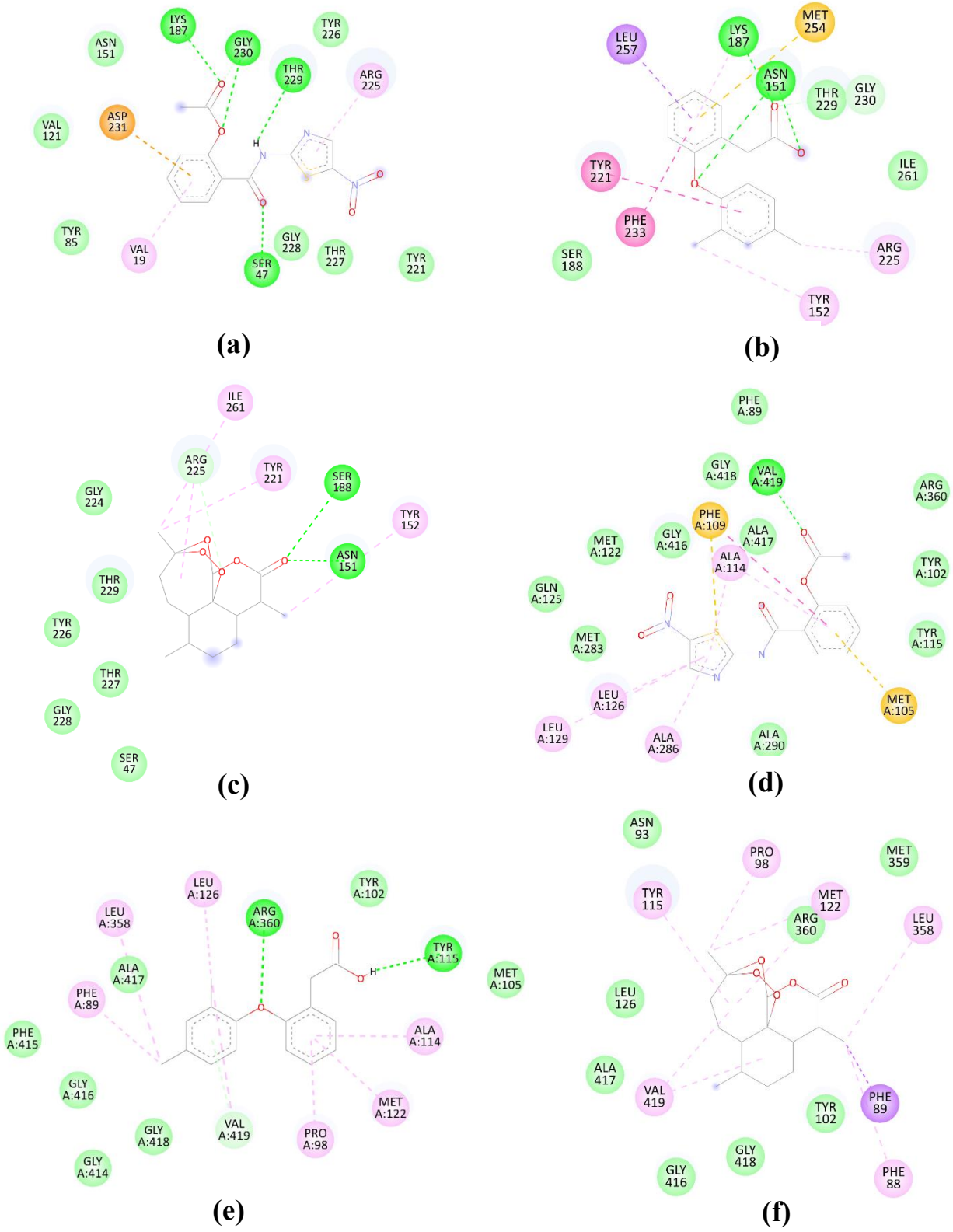

Figure 4.2: Docked structure of PK with Lig_1(a), Lig_2(b), Lig_3(c) and SDM with Lig_1(d), Lig_2(e) and Lig_3(f) interactions. The interactions present are van der Waals bonds (cyan), H-bonds (green), π-σ bonds (purple), and alkyl bonds (pink).

4.4.4. MD simulations: trajectory analyses

To understand the behavior of proteins under different conditions, including the presence and absence of chemical molecules, MD simulations are utilized. This method involves simulating various molecular systems over time to observe time-dependent phenomena. In the context of assessing drug molecules, Lig_1 [Nitazoxanide (PubChem ID-41684)], Lig_2 [Fenclofenac (PubChem ID-65394)] and Lig_3 [Artemisinin (PubChem ID-68827)] with each PK and SDM proteins were selected from the above analysis along with PK apo and SDM apo as control. Out of the three selected ligands, Lig_3(PubChem ID-68827) obtained from the Chinese medicinal plant, *Artemisia annua* and were used in malaria treatment [51]. Thus, providing evidence of phytochemical using as drugs. For complex systems of both targets, we have taken the simulated proteins. We considered the optimal complex conformation based on the docking data and proceeded with 100 ns simulations for each system. Trajectory analyses were conducted, including methods such as Root Mean Square Deviation (RMSD), which measures the variation between the initial and final structural conformations of a protein's backbone. Additionally, Root Mean Square Fluctuation (RMSF) was used to determine the average movement of individual protein residues relative to a reference point over the simulation period. Furthermore, Radius of Gyration (Rg) was employed to provide insights into the arrangement of protein atoms along its axis during the simulation timeframe.

4.4.5. Structure change analysis

Analyzing the structural changes is crucial for providing a clearer understanding of how protein structures evolve during the simulation process while interacting with the selected ligands. In the case of PK, the snapshots of PK-Lig_1 demonstrated minimal structural alterations, indicating sustained stability throughout the simulation. Conversely, PK-Lig_2 and PK-Lig_3 exhibited modest modifications, as depicted in Figure 4.3.1. On the other hand, Figure 4.3.2 illustrated that the structures of SDM-Lig_1, SDM-Lig_2, and SDM-Lig_3 underwent changes in certain regions. Despite these changes, the stability of the complexes remained unaffected. Consequently, all complex structures of both proteins exhibited consistent and stable conformations.

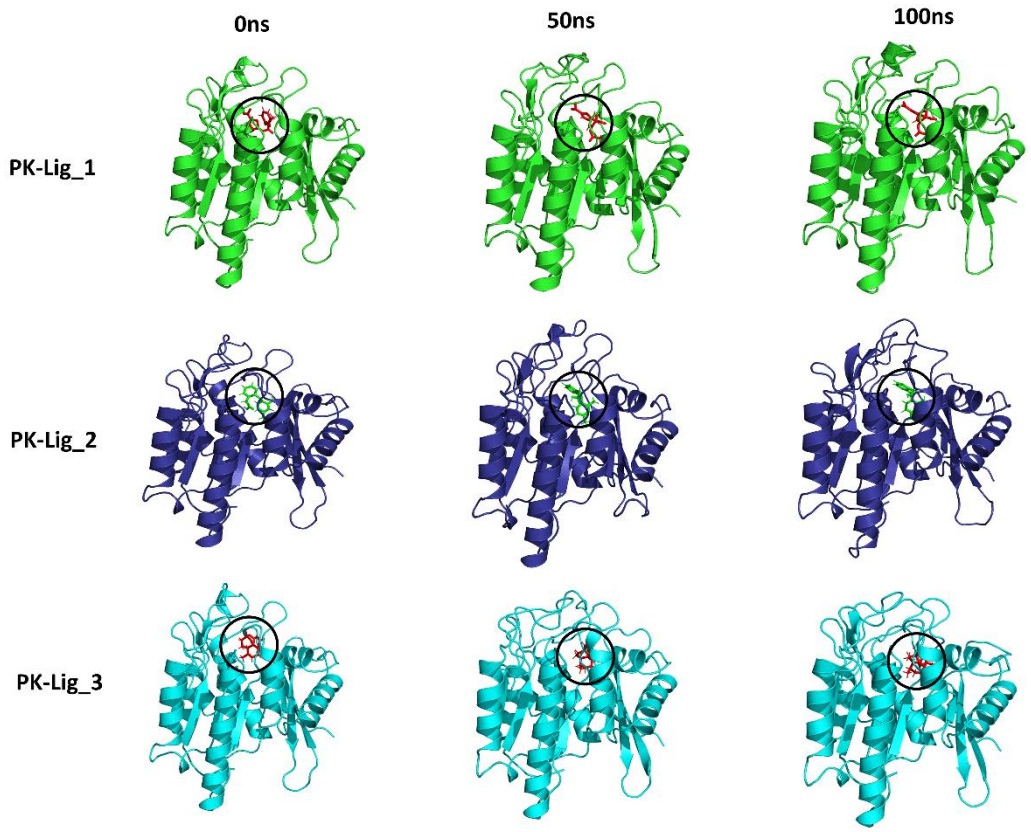

Figure 4.3.1: Representation of PK with Lig_1, Lig_2 and Lig_3 at 0 ns, 50 ns and 100 ns of MD simulation.

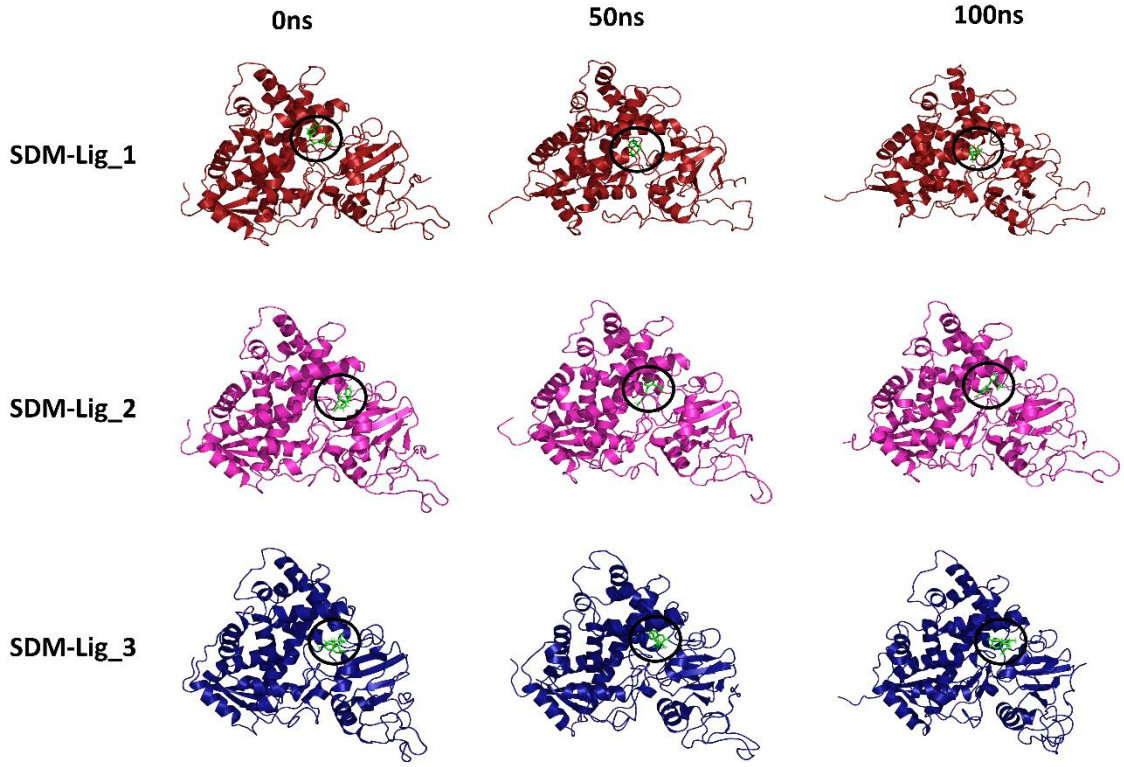

Figure 4.3.2: Representation of SDM with Lig_1, Lig_2 and Lig_3 at 0 ns, 50 ns and 100 ns of MD simulation.

4.4.6. Stability analysis

The RMSD plots of both the protein backbone were shown in the presence and absence of ligands. Regarding PK, the analysis of the apo structure indicated significant fluctuation in RMSD, spanning from 0.27 to 0.4 nm, before stabilizing after 80ns. On the other hand, the PK-Lig_1 and PK-Lig_2 complexes reached equilibrium promptly after 50ns. In contrast, the PK-Lig_3 system displayed continuous fluctuations throughout the entirety of the simulation period. The cumulative RMSD of PK-Lig_1 and PK-Lig_2 was below 0.27 nm than others. In the systems of SDM, the stability of ligand-free SDM showed high fluctuations. The RMSD plot patterns for both SDM-Lig_1 and SDM-Lig_2 remained within the range of 0.2-0.3 nm. Notably, Lig_1 and Lig_2 exhibited comparable trends in their fluctuations, which were notably lower compared to the fluctuations observed in the control protein graph. From Figure 4.4, we observed that the targets obtained more stability when bound to Lig_1 and Lig_2, which controlled the dynamic behavior of protein backbones at 0.3 nm.

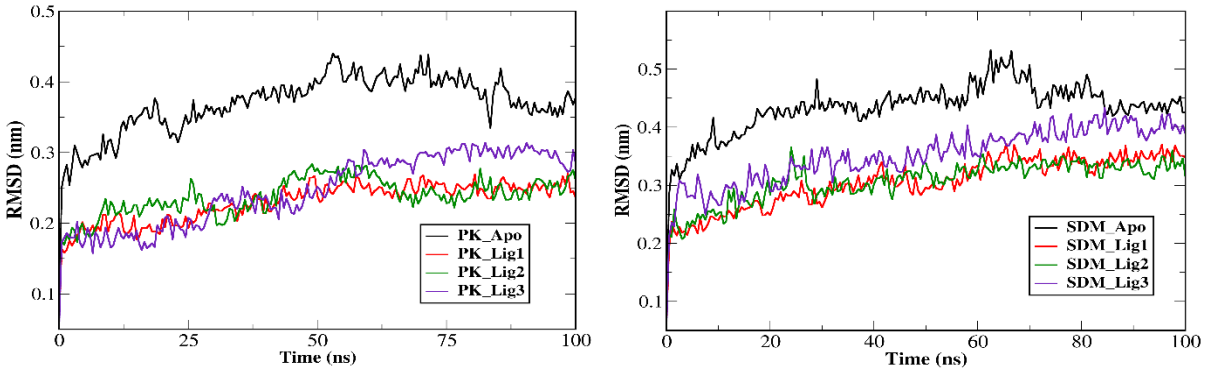

Figure 4.4: RMSD plot of PK-apo, SDM-apo and complexes with selected ligands.

4.4.7. Residue fluctuation analysis

To explore the flexibility of residues within both proteins under various conditions, both with and without ligands, RMSF analysis was conducted. For PK systems, the analysis of residue-wise fluctuations revealed similar trends between the apo-PK and the PK forms bound to different ligands. The RMSF graph representing the flexibility of the PK protein was created and depicted in Figure 4.5. In the case of SDM protein, the ligand unbound SDM system showed some fluctuations between 13-17, 210-215 and 452-456 residues. Similarly, SDM-Lig_3 showed fluctuations between 45-50, 140-160 and 390-400 regions. Both apo-SDM and SDM-Lig_3 affect the structural integrity of the structure. Contrariwise,

the analysis showed that the binding of Lig_1 and Lig_2 reduced fluctuations of SDM backbone atoms compared with Lig_3.

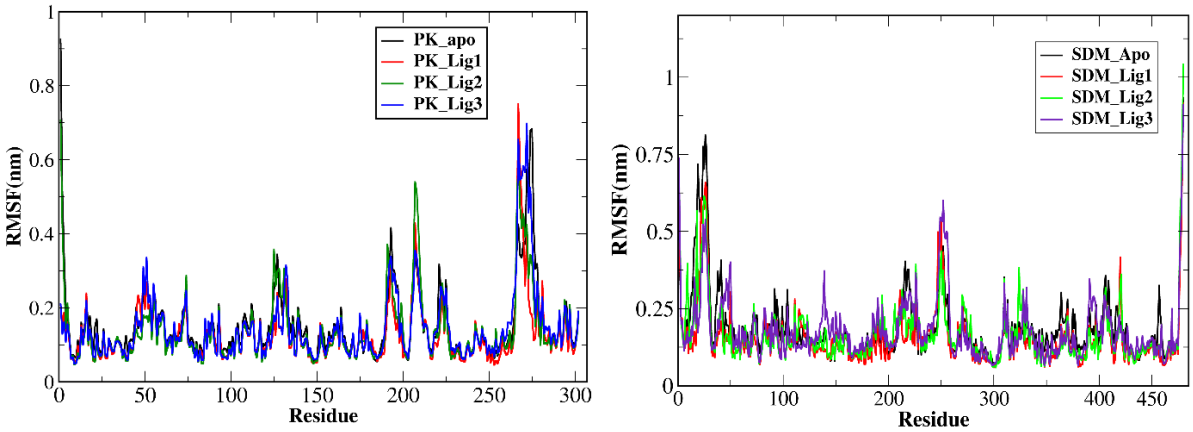

Figure 4.5: RMSF plot of PK-apo, SDM-apo and complexes with selected ligands

4.4.8. Radius of gyration analysis

To gain insight into the protein's compactness during the simulation, Rg (Radius of Gyration) parameter is used. In the part of PK system, PK-apo shows fluctuations throughout the simulations in contrast to the ligand-bound protein which showed lesser fluctuations and more compactness. Within the set of complexes, Lig_1 demonstrated a stable behavior after 50ns of the simulation run. Analyzing the Rg of the SDM system revealed that the apo-SDM experienced fluctuations in the initial quarter of the simulation. Additionally, SDM-Lig_3 exhibited fluctuations from 75ns until the end of the simulation. In contrast, both SDM-Lig_1 and SDM-Lig_2 displayed stability from 15ns to the completion of the 100ns simulation, indicating a compact conformation in the presence of the ligands. From Figure 4.6, Rg analysis correlated with similar trends to those of RMSD and RMSF data.

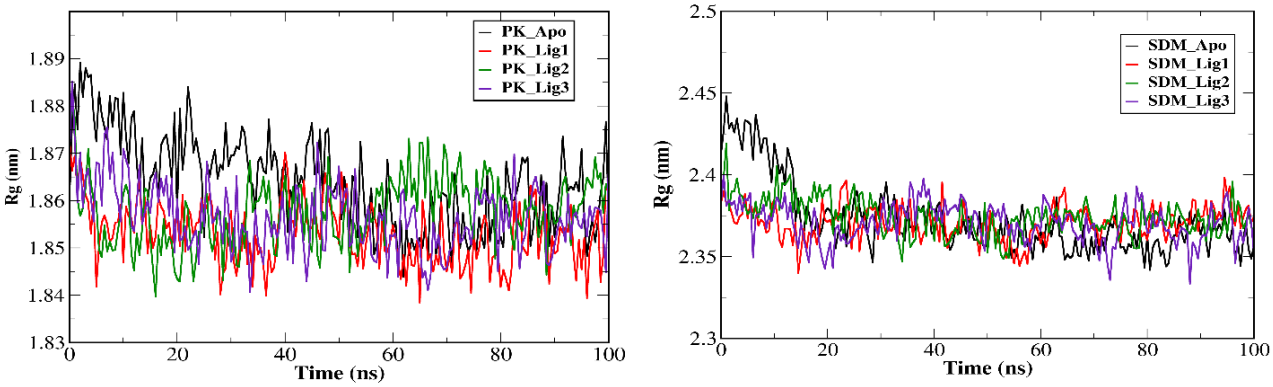

Figure 4.6: Radius of gyration plot of PK-apo, SDM-apo and complexes with selected ligands.

4.4.9. Hydrogen bond interaction analysis

Hydrogen-bond interactions calculation offers insight into the quality of interactions between ligands and the targeted proteins. To perform this analysis, we employed the gmx hbond command. Throughout the 100ns molecular dynamics simulations, hydrogen bonds were assessed between the proteins and their respective ligand systems within a solvent environment. The purpose was to verify the stability of these interactions. As depicted in Figure 4.6, when PK was bound to Lig_1, a range of 1 to 4 hydrogen bonds were observed up to the 50ns mark. Subsequently, the number of hydrogen bonds increased to 3 to 6 and remained consistent until the end of the simulation. In contrast, the PK-Lig_2 complex maintained a relatively stable count of 1 to 3 hydrogen bonds throughout the entire simulation. However, the number of H-bonds in the PK-Lig_2 was 1-3 throughout the simulation. It was observed that the Lig_1 binds with PK through hydrogen bonds with an average number of 4. In the case of SDM, it can be noted that SDM when bound to Lig_1 displayed 1-4 H-bonds after 30ns of simulation run whereas the SDM-Lig_2 complex showed 0-2 H-bonds and SDM-Lig_3 ranges in an average of 0-1 H-bonds. Our aforementioned findings provide evidence that Lig_1 can bind to both proteins with a greater number of H-bonds compared to the other selected ligands.

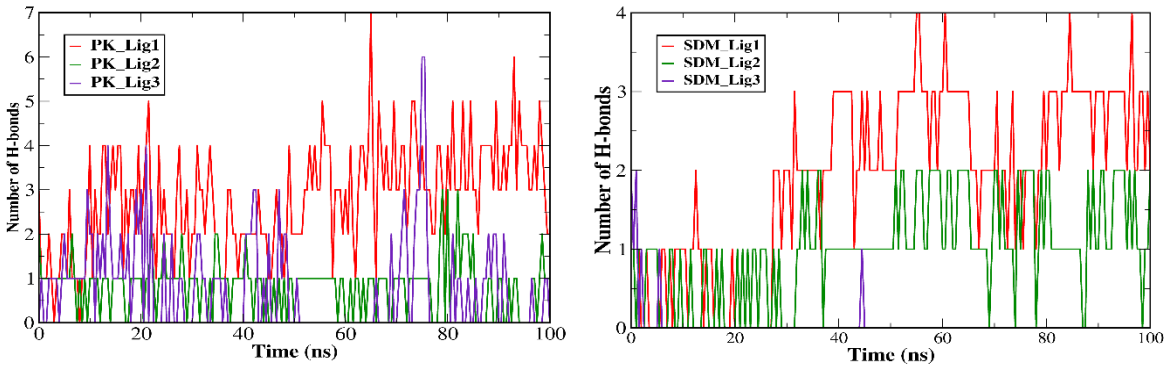

Figure 4.7: Hydrogen bond interaction plot of PK and SDM with selected ligands.

4.4.10. Non-bonded analysis

Following additional simulation analyses, we have made an effort to pinpoint the various non-bonded contacts that have contributed to the stability of both protein complexes during the course of the simulation. All over the simulation period, hydrophobic contacts, van der Waals contacts, and hydrogen bonds were discovered to be the most prevalent contacts between complexes. We assessed the count of nonbonded contacts across all the complexes during the entire simulation period. These interactions of all complexes were illustrated in

Figures 4.8.1 and 4.8.2. The number of interactions within each complex was tallied and is detailed in Table 4.6. Notably, among all the complexes, PK-Lig_1 and SDM-Lig_1 exhibited a higher number of hydrogen bonds and van der Waals interactions compared to hydrophobic interactions (such as Pi-hydrophobic, Pi-alkyl, and alkyl interactions).

Table 4.6: The number of non-bonded contacts between proteins (PK and SDM) and selected molecules

System	Time (ns)	HB	vdW	HC	TNB
PK-Lig_1	0	7	6	0	13
	50	3	12	0	15
	100	8	9	1	18
PK-Lig_2	0	3	6	3	12
	50	1	13	3	17
	100	2	9	6	17
PK-Lig_3	0	1	10	0	11
	50	0	10	5	15
	100	0	6	5	11
SDM-Lig_1	0	1	11	4	16
	50	3	12	2	17
	100	4	15	3	22
SDM-Lig_2	0	2	7	6	15
	50	1	7	7	15
	100	0	12	5	17
SDM-Lig_3	0	0	9	5	14
	50	0	10	8	18
	100	0	5	10	15

The representation in table 4.5 is H-bond (HB), van der Waals (vdW), Hydrophobic contacts (HC) and total non-bonded contacts (TNB).

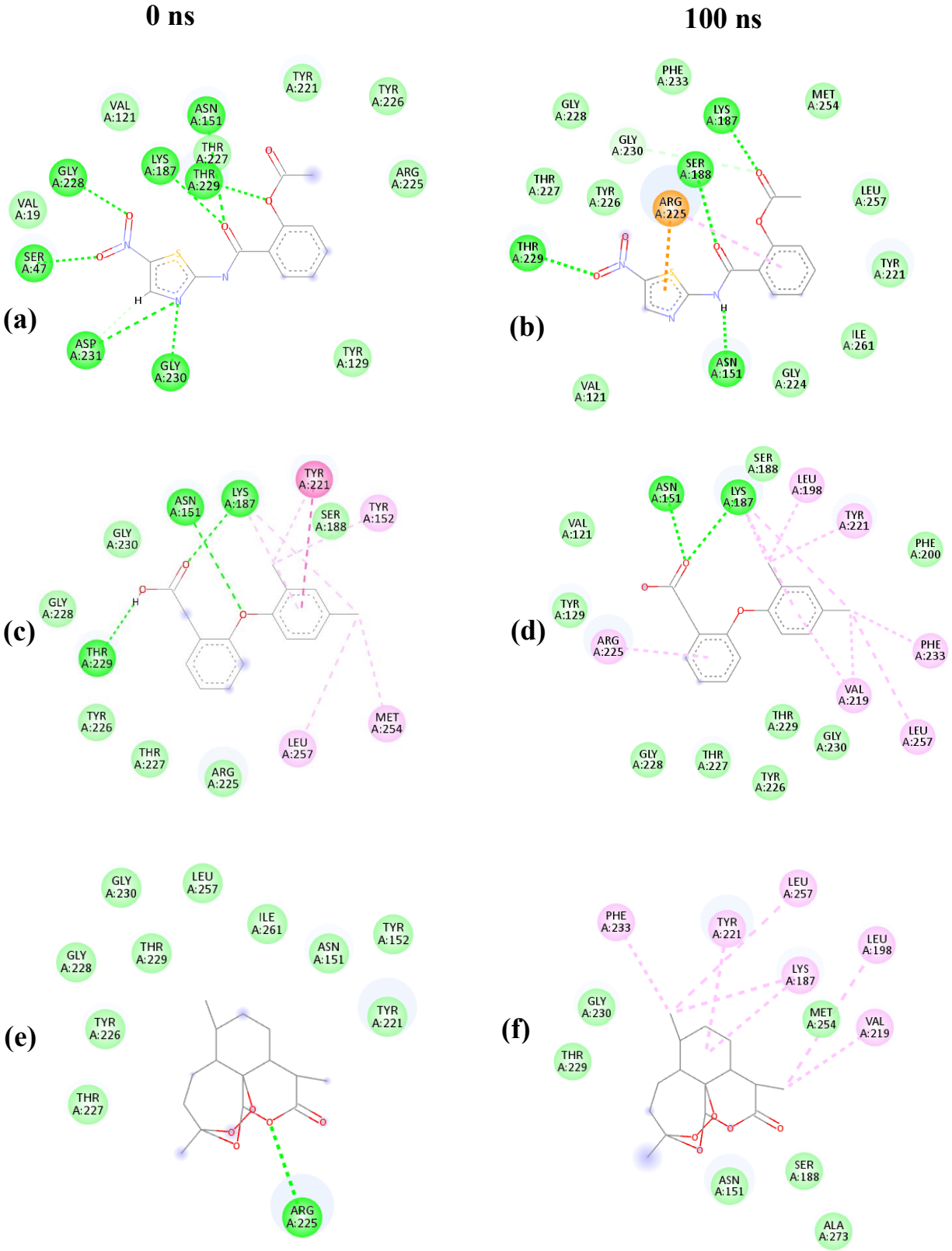

Figure 4.8.1: 2D visualization of PK using Lig_1(a,b), Lig_2(c,d), and Lig_3(e,f) at simulation times of 0 ns and 100 ns. van der Waals (cyans), H-bond (green), pi-sigma (purple), and alkyl interactions are all present (pink).

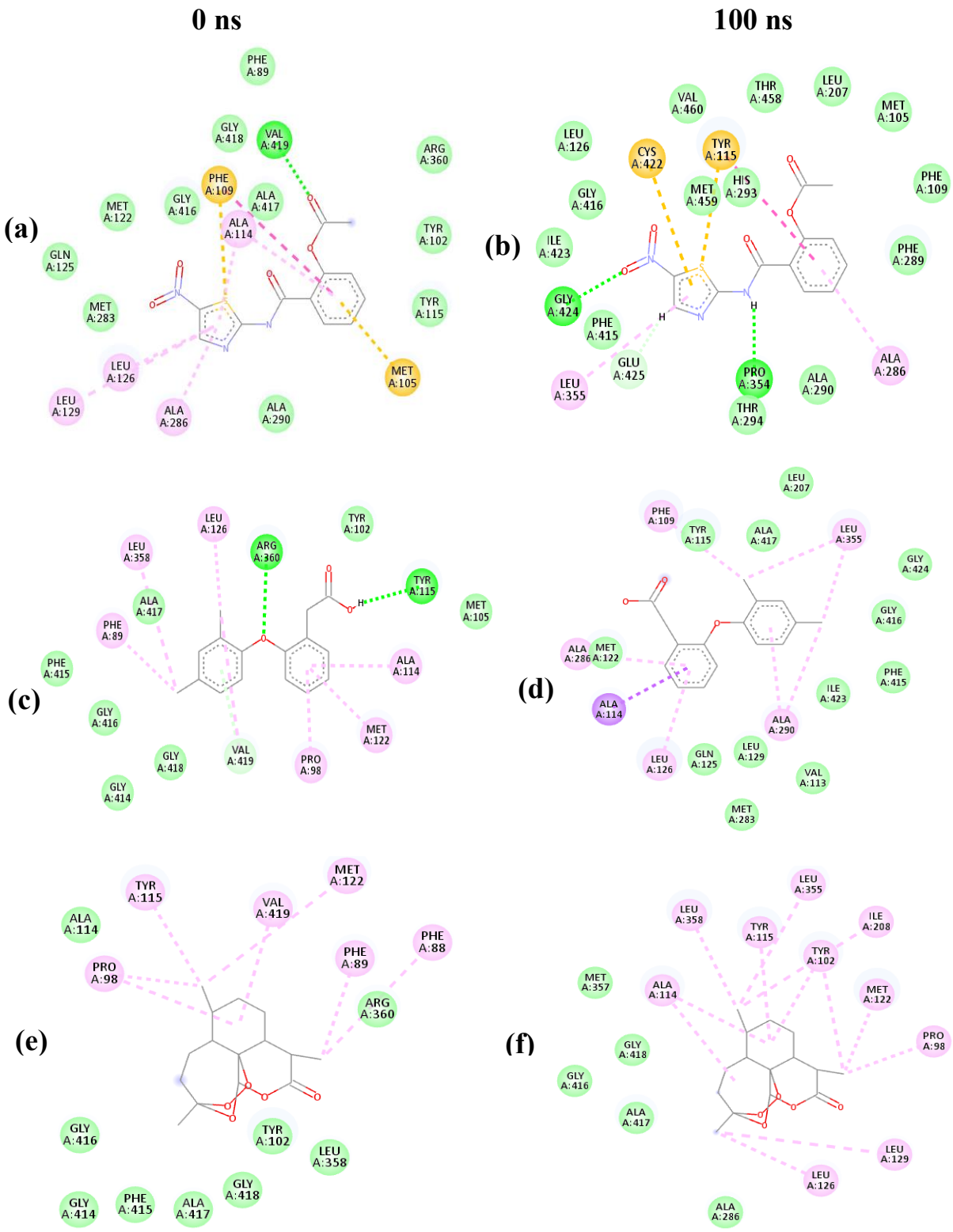

Figure 4.8.2: 2D visualization of SDM using Lig_1(a,b), Lig_2(c,d), and Lig_3(e,f) simulation times of 0 ns and 100 ns. Van der Waals (cyans), H-bond (green), pi-sigma (purple), and alkyl interactions are all present (pink).

4.5. MMPBSA and binding free energy analysis

To understand the molecular interaction of ligands with targets, the molecular mechanics/Poisson-Boltzmann surface area (MMPBSA) technique was applied for PK and SDM targets. MMPBSA was determined by retrieving the frames from the last 20 ns (each 200ps) of 100ns simulation. In order to calculate the binding free energies, we used the MMPBSA method found in the g_mmpbsa program.

Furthermore, Table 4.7 demonstrates that despite the modest contribution from G_{pol} (149.758 kJ/mol), the assessed binding free energy ($G_{Binding}$) for SDM-Lig_1 stands out as the highest (-175.609 kJ/mol) among all protein-ligand systems. Notably, the binding energy of SDM-Lig_1 is primarily influenced by electrostatic energy (-127.998 kJ/mol) and van der Waals energy (-180.693 kJ/mol). On the contrary, SDM-Lig_2 and SDM-Lig_3 exhibit lower binding energies. This discrepancy can be attributed to the relatively unfavorable contributions from G_{vdW} and G_{elec}, which hinder the provision of binding energy. In the context of PK, PK-Lig_1 and PK-Lig_3 exhibit comparable binding energies of -100.712 and -101.792 kJ/mol, respectively. The main contribution of binding energy for PK-Lig_1 is provided by the electrostatic energy (-142.437 kJ/mol) whereas in PK-Lig_3 the major addition is done by the van der Waals energy (-151.646 kJ/mol). In comparison to other molecules binding to their respective targets, PK-Lig_1 (-142.437 kJ/mol) and SDM-Lig_1 (-127.998 kJ/mol) contributed much more electrostatic energy to the total binding energy. Along with MD simulation analysis, the $G_{Binding}$ may provide support for better affinities of molecules towards relevant PK and SDM targets.

Table 4.7: Average MMPBSA energy (kJ/mol) for the binding of PK and SDM with selected ligands

System	PK-Lig_1	PK-Lig_2	PK-Lig_3	SDM-Lig_1	SDM-Lig_2	SDM-Lig_3
$G_{Binding}$ (w+x+y+z)	-100.71 ± 22.01	-73.23 ± 30.80	-101.79 ± 18.97	-175.61 ± 12.64	-131.93 ± 12.73	-125.25 ± 12.91
G_{vdW} (w)	-140.05 ± 11.42	-139.33 + 12.04	-151.65 ± 11.1	-180.69 ± 10.31	-148.98 ± 9.81	-154.39 ± 8.41
G_{elec} (x)	-142.44 ± 24.45	-78.86 + 27.86	-77.00 ± 22.28	-127.99 ± 16.79	-39.95 ± 15.64	-46.47 ± 9.44

G_{pol} (y)	197.61 ± 15.19	162.21 + 22.12	142.00 ± 19.36	149.76 ± 9.53	75.32 ± 8.30	91.74 ± 9.20
G_{SASA} (z)	-15.83 ± 0.71	-17.25 + 0.99	-15.15 ± 0.73	-16.68 ± 0.72	-18.32 ± 0.89	-16.13 ± 0.68

4.6. Discussion

Creating an effective drug against VL presents substantial hurdles, given the resistance and adverse effects encountered by existing drugs [52]. Consequently, the quest for novel drug compounds to address VL becomes imperative. Additionally, there has been a noticeable surge in VL-related fatalities, prompting the utilization of computational methods in this study to impede the proliferation of *L. donovani*. This critical situation compelled us to identify crucial genes suitable for targeting and subsequently screen drug molecules against them as potential remedies. The indispensability of both PK and SDM proteins for the survival of *L. donovani* has been uncovered, as they perform essential functions necessary for the organism's viability. The interest on drugs obtained from most of the plants and their alternatives has increased over the years in various countries [53]. Our study's primary goal was to demonstrate use of different drugs which are collected from databases against the specific protein targets (PK and SDM). We aimed to determine whether the binding of these drugs could lead to stabilization and induce alterations in their characteristics. The study encompassed a series of screening steps, involving the selection of drug targets, refinement of drug candidates, and subsequent employment of computational tools such as molecular docking, MD simulations, and the MMPBSA technique [54]. However, ADMET study is not performed for the compounds taken for the work because the compounds are already considered as drugs and have gone through different clinical trials. Initially, molecular docking was used to determine the possible therapeutic candidate for the chosen proteins by calculating the ligand's binding affinity to the target protein. After evaluating the binding affinity of a common set of 10 ligands against both protein targets using AutoDock 4.2, we selected three ligand molecules that demonstrated promising attributes based on PASS analysis, docking scores, and established applications. These three chosen ligands are Lig_1 (Nitazoxanide, PubChem ID-41684), Lig_2 (Fenclofenac, PubChem ID-65394), and Lig_3 (Artemisinin, PubChem ID-68827). Notably, these ligands have been predicted to exhibit antileishmanial activities. Furthermore, within this trio of ligands, Lig_1 and Lig_3 have

been shown to possess antileishmanial properties through *in vitro* and *in vivo* studies. [55-57].

To evaluate the enduring nature of the interactions, MD simulations were conducted. These simulations are instrumental in scrutinizing the dynamic conformational changes of biomolecules within systems comprised of proteins and ligands. Subsequently, the intermolecular forces stemming from interactions within protein-ligand complexes were investigated and examined through the analysis of simulated data.

The unique aspect of our work is the choice of drug targets from two separate protein data sets and to identify common targets, as well as the screening of medications using predictions of their anti-parasitic effects [8]. In addition, stability and accurate confirmation between the ligand and protein are required to influence the function of protein. In the initial phase, MD simulation was performed for the two chosen proteins (apo) then three compounds bound to the protein for each target were performed for 100ns. The conformational dynamics of the protein-ligand complexes were revealed through the analysis of Root Mean Square Deviation (RMSD) and Radius of Gyration (Rg). In comparison to the ligand-bound complexes, the unbound apo proteins of both PK and SDM exhibited fluctuations in RMSD and Rg. This observation suggests that the presence of ligands contributes to stabilizing both proteins. Upon scrutinizing the trajectories obtained from the MD simulation runs, Lig_1 and Lig_2 demonstrated noteworthy stability when interacting with the selected targets. However, Lig_1 exhibited higher stability with both PK and SDM compared to Lig_2 and Lig_3. This is indicated by the higher number of hydrogen bonds sustained throughout the simulation, indicating that Lig_1 offers enhanced stability to both proteins. The MD simulations analysis verifies that PK forms hydrogen bonds with Lig_1 through specific protein residues, namely Asn151, Lys187, Ser188, and Thr229. On the other hand, SDM maintains stable interactions with Lig_1 by establishing two hydrogen bonds with Pro354 and Gly424 during the MD simulation. The non-bonded interactions study between the two selected targets and compounds showed that there were other interactions besides H-bonds that aid protein active site residues in binding to the molecules. Besides H-bonds, other contacts include van der Waals interaction and hydrophobic contacts which also contributes to better stability. Among the three ligands selected, Lig_1 and Lig_3 with two targets performed better results in different MD simulation analyses.

To reinforce the previously obtained results, MMPBSA analysis was conducted in tandem with the MD simulation. This approach involved assessing various factors that collectively contributed to the overall binding energy of the drugs with the proteins. SDM-Lig_1 was shown to have the highest binding of all the complexes, and PK-Lig_1 and PK-Lig_3 showed similar total binding energies. However, the contribution of electrostatic energy was high in the case of Lig_1 with the PK making it more evident in providing stability.

The integrated utilization of computational compound screening, molecular docking, molecular dynamics simulations, and MMPBSA analysis aids in the identification of appropriate drug targets (PK and SDM) and potential inhibitors. This comprehensive approach is aimed at effectively impeding the progression of pathogenesis.

Bibliography

[1] Croft, S. L. and Coombs, G. H. Leishmaniasis–current chemotherapy and recent advances in the search for novel drugs. *Trends in parasitology*, 19(11):502-508, 2003.

[2] Fernandes, F. R., Ferreira, W. A., Campos, M. A., Ramos, G. S., Kato, K. C., Almeida, G. G. ... and Frézard, F. Amphiphilic antimony (V) complexes for oral treatment of visceral leishmaniasis. *Antimicrobial agents and chemotherapy*, 57(9):4229-4236, 2013.

[3] Ready, P. D. Biology of phlebotomine sand flies as vectors of disease agents. *Annual review of entomology*, 58:227-250, 2013.

[4] Singh, S., Sarma, S., Katiyar, S. P., Das, M., Bhardwaj, R., Sundar, D. and Dubey, V. K. Probing the molecular mechanism of hypericin-induced parasite death provides insight into the role of spermidine beyond redox metabolism in Leishmania donovani. *Antimicrobial agents and chemotherapy*, 59(1):15-24, 2015.

[5] eBioMedicine. Leishmania: An urgent need for new treatments. *EBioMedicine*, 87(104440): 2023.

[6] Rajkhowa, S., Hazarika, Z. and Jha, A. N. Systems biology and bioinformatics approaches in leishmaniasis. In *Applications of Nanobiotechnology for Neglected Tropical Diseases* (pp. 509-548). Academic Press, 2021.

[7] Bora, N. and Jha, A. N. In silico metabolic pathway analysis identifying target against leishmaniasis–a kinetic modeling approach. *Frontiers in Genetics*, 11:481222, 2020.

[8] Saha, D. and Nath Jha, A. Computational multi-target approach to target essential enzymes of Leishmania donovani using comparative molecular dynamic simulations and MMPBSA analysis. *Phytochemical Analysis*, 34(7):842-854, 2023.

[9] Bora, N. and Nath Jha, A. An integrative approach using systems biology, mutational analysis with molecular dynamics simulation to challenge the functionality of a target protein. *Chemical biology & drug design*, 93(6):1050-1060, 2019.

[10] Indari, O., Singh, A. K., Tiwari, D., Jha, H. C. and Jha, A. N. Deciphering antiviral efficacy of malaria box compounds against malaria exacerbating viral pathogens-Epstein Barr virus and SARS-CoV-2, an in silico study. *Medicine in Drug Discovery*, 16:100146, 2022.

[11] Jha, A. N. Computational approaches to build therapeutic paradigms targeting genes, proteins and pathways against neglected tropical diseases (NTDs). *Frontiers in Genetics*, 14:1183034, 2023.

[12] Zhang, C., Zheng, W., Cheng, M., Omenn, G. S., Freddolino, P. L. and Zhang, Y. Functions of essential genes and a scale-free protein interaction network revealed by structure-based function and interaction prediction for a minimal genome. *Journal of proteome research*, 20(2):1178-1189, 2021.

[13] Jakhmola, S., Hazarika, Z., Jha, A. N. and Jha, H. C. In silico analysis of antiviral phytochemicals efficacy against Epstein–Barr virus glycoprotein H. *Journal of Biomolecular Structure and Dynamics*, 40(12):5372-5385, 2022.

[14] Kumari, I., Lakhanpal, D., Swargam, S. and Nath Jha, A. Leishmaniasis: Omics approaches to understand its biology from molecule to cell level. *Current Protein and Peptide Science*, 24(3):229-239, 2023.

[15] Rather, M. A., Saha, D., Bhuyan, S., Jha, A. N. and Mandal, M. Quorum quenching: a drug discovery approach against Pseudomonas aeruginosa. *Microbiological Research*, 264:127173, 2022.

[16] Santos, R., Ursu, O., Gaulton, A., Bento, A. P., Donadi, R. S., Bologa, C. G., ... and Overington, J. P. A comprehensive map of molecular drug targets. *Nature reviews Drug discovery*, 16(1):19-34, 2017.

[17] Singh, B. K., Sarkar, N., Jagannadham, M. V. and Dubey, V. K. Modeled structure of trypanothione reductase of Leishmania infantum. *BMB reports*, 41(6):444-447, 2008.

[18] Eliot, A. C. and Kirsch, J. F. Pyridoxal phosphate enzymes: mechanistic, structural, and evolutionary considerations. *Annual review of biochemistry*, 73(1):383-415, 2004.

[19] Parletta, N., Milte, C. M. and Meyer, B. J. Nutritional modulation of cognitive function and mental health. *The Journal of nutritional biochemistry*, 24(5):725-743, 2013.

[20] Kumar, V., Sharma, M., Rakesh, B. R., Malik, C. K., Neelagiri, S., Neerupudi, K. B., ... and Singh, S. Pyridoxal kinase: a vitamin B6 salvage pathway enzyme from Leishmania donovani. *International journal of biological macromolecules*, 119:320-334, 2018.

[21] Jones, D. C., Alphey, M. S., Wyllie, S. and Fairlamb, A. H. Chemical, genetic and structural assessment of pyridoxal kinase as a drug target in the African trypanosome. *Molecular microbiology*, 86(1):51-64, 2012.

[22] Oliveira-da-Silva, J. A., Machado, A. S., Ramos, F. F., Tavares, G. S., Lage, D. P., Ludolf, F., ... & Coelho, E. A. (2020). Evaluation of Leishmania infantum pyridoxal kinase protein for the diagnosis of human and canine visceral leishmaniasis. *Immunology Letters*, *220*, 11-20.

[23] Kronenberger, T., Lindner, J., Meissner, K. A., Zimbres, F. M., Coronado, M. A., Sauer, F. M., ... and Wrenger, C. Vitamin B6-dependent enzymes in the human malaria parasite Plasmodium falciparum: a druggable target?. *BioMed Research International*, 2014.

[24] Are, S., Gatreddi, S., Jakkula, P. and Qureshi, I. A. Structural attributes and substrate specificity of pyridoxal kinase from Leishmania donovani. *International journal of biological macromolecules*, 152:812-827, 2020.

[25] Volkman, J. K. Sterols and other triterpenoids: source specificity and evolution of biosynthetic pathways. *Organic geochemistry*, 36(2):139-159, 2005.

[26] I Lepesheva, G. and R Waterman, M. Sterol 14alpha-demethylase (CYP51) as a therapeutic target for human trypanosomiasis and leishmaniasis. *Current topics in medicinal chemistry*, 11(16):2060-2071, 2011.

[27] Ghosh, M., Roy, K., Das Mukherjee, D., Chakrabarti, G., Roy Choudhury, K. and Roy, S. Leishmania donovani infection enhances lateral mobility of macrophage membrane protein which is reversed by liposomal cholesterol. *PLoS neglected tropical diseases*, 8(12):e3367, 2014.

[28] Yao, C. and Wilson, M. E. Dynamics of sterol synthesis during development of Leishmania spp. parasites to their virulent form. *Parasites & vectors*, 9:1-12, 2016.

[29] McCall, L. I., El Aroussi, A., Choi, J. Y., Vieira, D. F., De Muylder, G., Johnston, J. B. ... and McKerrow, J. H. Targeting ergosterol biosynthesis in Leishmania donovani: essentiality of sterol 14alpha-demethylase. *PLoS neglected tropical diseases*, 9(3):e0003588, 2015.

[30] Sakyi, P. O., Kwofie, S. K., Tuekpe, J. K., Gwira, T. M., Broni, E., Miller III, W. A. ... and Amewu, R. K. Inhibiting Leishmania donovani sterol methyltransferase to identify lead compounds using molecular modelling. *Pharmaceuticals*, 16(3):330, 2023.

[31] Xu, W., Hsu, F. F., Baykal, E., Huang, J. and Zhang, K. Sterol biosynthesis is required for heat resistance but not extracellular survival in Leishmania. *PLoS pathogens*, 10(10):e1004427, 2014.

[32] Shakya, A. K. Medicinal plants: Future source of new drugs. *International journal of herbal medicine*, 4(4):59-64, 2016.

[33] Rose, Y., Duarte, J. M., Lowe, R., Segura, J., Bi, C., Bhikadiya, C.... and Westbrook, J. D. RCSB Protein Data Bank: architectural advances towards integrated searching and efficient access to macromolecular structure data from the PDB archive. *Journal of molecular biology*, 433(11):166704, 2021.

[34] Webb, B. and Sali, A. Protein structure modeling with MODELLER. *Functional genomics: Methods and protocols*, 39-54, 2017.

[35] Wishart, D. S., Knox, C., Guo, A. C., Cheng, D., Shrivastava, S., Tzur, D.... and Hassanali, M. DrugBank: a knowledgebase for drugs, drug actions and drug targets. *Nucleic acids research*, 36(suppl_1):D901-D906, 2008.

[36] Avram, S., Bologa, C. G., Holmes, J., Bocci, G., Wilson, T. B., Nguyen, D. T.... and Oprea, T. I. DrugCentral 2021 supports drug discovery and repositioning. *Nucleic acids research*, 49(D1):D1160-D1169, 2021.

[37] Kim, S., Thiessen, P. A., Bolton, E. E., Chen, J., Fu, G., Gindulyte, A.... and Bryant, S. H. PubChem substance and compound databases. *Nucleic acids research*, 44(D1):D1202-D1213, 2016.

[38] O'Boyle, N. M., Banck, M., James, C. A., Morley, C., Vandermeersch, T. and Hutchison, G. R. Open Babel: An open chemical toolbox. *Journal of cheminformatics*, 3:1-14, 2011.

[39] Lagunin, A., Stepanchikova, A., Filimonov, D. and Poroikov, V. PASS: prediction of activity spectra for biologically active substances. *Bioinformatics*, 16(8):747-748, 2000.

[40] Saha, D. and Jha, A. N. Multi-target approach on Leishmania donovani and finding out potent inhibitors for essential enzymes. In *Proceedings of the XXXVIII Symposium of Bioinformatics and Computer-Aided Drug Discovery pp*, 2022.

[41] Lyndem, S., Hazarika, U., Athul, P., Bhatta, A., Prakash, V., Jha, A. N. and Roy, A. S. A comprehensive in vitro exploration into the interaction mechanism of coumarin derivatives with bovine hemoglobin: Spectroscopic and computational methods. *Journal of Photochemistry and Photobiology A: Chemistry*, 436:114425, 2023.

[42] Abraham, M. J., Murtola, T., Schulz, R., Páll, S., Smith, J. C., Hess, B. and Lindahl, E. GROMACS: High performance molecular simulations through multi-level parallelism from laptops to supercomputers. *SoftwareX*, 1:19-25, 2015.

[43] Kumari, R., Kumar, R., Open Source Drug Discovery Consortium and Lynn, A. g_mmpbsa□ A GROMACS tool for high-throughput MM-PBSA calculations. *Journal of chemical information and modeling*, 54(7):1951-1962, 2014.

[44] Gupta, R., Kumar, V., Kushawaha, P. K., Tripathi, C. P., Joshi, S., Sahasrabuddhe, A. A., ... and Dube, A. Characterization of glycolytic enzymes-rAldolase and rEnolase of Leishmania donovani, identified as Th1 stimulatory proteins, for their

immunogenicity and immunoprophylactic efficacies against experimental visceral leishmaniasis. *Plos one*, *9*(1): e86073, 2014

[45] Colotti, G. and Ilari, A. Polyamine metabolism in Leishmania: from arginine to trypanothione. *Amino acids*, 40(2):269-285, 2011

[46] Sheikh, S. Y., Hassan, F., Shukla, D., Bala, S., Faruqui, T., Akhter, Y., ... and Nasibullah, M. A review on potential therapeutic targets for the treatment of leishmaniasis. *Parasitology International*, 102863, 2024

[47] Boitz, J. M., Yates, P. A., Kline, C., Gaur, U., Wilson, M. E., Ullman, B. and Roberts, S. C. Leishmania donovani ornithine decarboxylase is indispensable for parasite survival in the mammalian host. *Infection and immunity*, 77(2):756-763, 2009

[48] Tiwari, K., Kumar, R. and Dubey, V. K. Biochemical characterization of dihydroorotase of Leishmania donovani: Understanding pyrimidine metabolism through its inhibition. *Biochimie*, 131:45-53, 2016

[49] Allen, T. E., Hwang, H. Y., Jardim, A., Olafson, R. and Ullman, B. Cloning and expression of the hypoxanthine-guanine phosphoribosyltransferase from Leishmania donovani. *Molecular and biochemical parasitology*, 73(1-2):133-143, 1995

[50] Phillips, M. A. Stoking the drug target pipeline for human A frican trypanosomiasis. *Molecular microbiology*, 86(1):10-14, 2012.

[51] Ikram, N. K. and Simonsen, H. T. A review of biotechnological artemisinin production in plants. *Frontiers in Plant Science*, 8:303099, 2017.

[52] Chanda, K. An overview on the therapeutics of neglected infectious diseases—Leishmaniasis and Chagas diseases. *Frontiers in Chemistry*, 9:622286, 2021.

[53] Lazarou, R. and Heinrich, M. Herbal medicine: Who cares? The changing views on medicinal plants and their roles in British lifestyle. *Phytotherapy research*, 33(9):2409-2420, 2019.

[54] Katiki, M., Sharma, M., Neetu, N., Rentala, M. and Kumar, P. Biophysical and modeling-based approach for the identification of inhibitors against DOHH from Leishmania donovani. *Briefings in Functional Genomics*, 22(2):217-226.

[55] Zhang, R., Shang, L., Jin, H., Ma, C., Wu, Y., Liu, Q., ... and Gao, H. In vitro and in vivo antileishmanial efficacy of nitazoxanide against Leishmania donovani. *Parasitology research*, 107:475-479, 2010.

[56] Verma, A., Ghosh, S., Salotra, P. and Singh, R. Artemisinin-resistant Leishmania parasite modulates host cell defense mechanism and exhibits altered expression of unfolded protein response genes. *Parasitology research*, 118:2705-2713, 2019.

[57] Ghaffarifar, F., Heydari, F. E., Dalimi, A., Hassan, Z. M., Delavari, M. and Mikaeiloo, H. Evaluation of apoptotic and antileishmanial activities of Artemisinin on promastigotes and BALB/C mice infected with Leishmania major. *Iranian journal of parasitology*, 10(2):258, 2015.